Experimental Investigation of Cylindrical Isolator with Mild Jet Injection Mass Flow Ratios

Sean Murray[1], Morgan Funderburk[2], and Venkateswaran Narayanaswamy[3]
Department of Mechanical and Aerospace Engineering,
North Carolina State University, Raleigh, NC 27695

Unstart of scramjet and ramjet engines may occur due to boundary layer separation caused by excessive downstream pressure build-up. Pressure is built up in the combustor primarily due to fuel mass addition, and combustion induced heat release. Significant experimental and computational efforts have focused on the characterization of the unstart process in rectangular isolators. By comparison, little literature exists regarding unstart in cylindrical isolators due to difficulties in imaging/measurement techniques associated with curvature. In the present work, preliminary experiments are conducted to investigate the mean and unsteady aspects of a cylindrical isolator with mild mass injection mass flow ratios, insufficient to induce unstart. A cylindrical isolator duct is explored at Re/m = 4.4 x 10^7 m^{-1} and M_∞ = 3.0. Surface streakline flow visualization and high-frequency wall static pressure measurements are used to evaluate the flowfield to provide an in-depth baseline case for comparative purposes once the model is unstarted in future studies. Comparison between cases with and without jet injection indicated a lack of upstream mean or unsteady influence due to the mild jet mass flow ratio. Consistency is seen between all measurement techniques, supporting the application of these methods in the evaluation of unstarted flow in future investigations.

Nomenclature

M	Mach number
u	Velocity, *m/s*
T	Temperature, *K*
Re	Reynolds number
p	Static pressure, *kPa*
γ	Specific heat ratio
$\dot{m}$	Mass flow rate, kg/s^{-1}
f	Frequency, *kHz*
G(f)	Power spectra
σ	Root mean square
x	Streamwise coordinate, *mm*
y	Vertical coordinate, *mm*
z	Transverse coordinate, *mm*

Subscript

w	Wall

[1] Undergraduate Research Assistant.
[2] Graduate Research Assistant.
[3] Assistant Professor.

jet	Jet
isolator	Isolator
∞	Freestream

I. Introduction

Ramjet and scramjet propulsion technologies are vital to the future of air-breathing hypersonic vehicles. Developments in high-speed propulsion systems have been obstructed by a flow phenomenon in the inlet/isolator of scramjets called unstart. The unstart process causes detrimental reductions in mass flow through the engine, large thermal/mechanical loads, and severe loss of thrust [1]. Unstart can abruptly impair vehicle operation as evidenced by the second test flight of the X-51 hypersonic vehicle [2]. Due to the limited knowledge surrounding unstart, the influencing factors, criteria for initiation, and process mechanisms must be fully understood before control strategies can be effectively explored.

The unstart process has been characterized by boundary layer separation induced by downstream blockages which generates an oblique or normal shock, known as the unstart shock system. This unstart shock system is then seen to propagate upstream following further downstream pressure rises, eventually pushing the unstart shock system out of the inlet, disgorging the original shock train [1]. An initiation phase has been reported in which peak unsteadiness is observed while the unstart shock system sits in the isolator, prior to the propagation phase, where in the unstart shock system is fully ejected from the inlet [3]. Following the ejection of the unstart shock, Wagner et al. [3] observed oscillation of the unstart shock in and out of the inlet. This perpetuation phase has been reported independent of downstream pressure rise mechanism [4, 5].

A large body of research both experimentally and computational has focused on characterizing the factors which influence the initiation of unstart [1, 3-10]. Im et al. [6] recently reviewed unstart literature and summarized the three main factors influencing unstart initiation as inlet/isolator geometry, incoming flow conditions, and the downstream pressure build-up. Downstream pressure build-up has been shown to primarily occur due to the fuel mass addition, and combustion-induced heat release occurring in the combustor. Multiple investigations have confirmed the coupled nature of mass injection and heat release and the inability to separate the two when considering unstart conditions [7]. Due to serious technical challenges regarding the reproduction of supersonic combustion in a laboratory setting, mass jet injection provides an alternative method for producing back pressure rise. Despite this, relatively few studies have used mass injection as the flow choking mechanism, with many instead using mechanical flow blockages, such as cylindrical pins [1]. Those studies which have explored mass injection induced unstart have primarily explored rectangular inlet and isolator geometries [6, 8, 9]. This provides ease of imaging techniques but is also less representative of actual scramjet design.

The present work aims to supplement current information on unstart induced by mass jet injection in rectangular geometries through an investigation of the flow characteristics of a cylindrical inlet/isolator model under mild jet injection mass flow ratios. The term “mild” here refers to mass flow rates less than those necessary to initiate unstart. The mass flow ratios investigated in this work span from no injection whatsoever to just below unstart levels, yielding data which will provide a basis for comparison when the unstart process is explored in a future work.

II. Experimental Setup

A. Facility

Table 1: Incoming flow characteristics.

Parameter	Value
M_∞	3.0
u_∞	630 m/s
T_∞	110 K
Re/m	4.4×10^7 m^{-1}
p_∞	16.8 kPa

All experiments were conducted in the North Carolina State University variable Mach number blowdown-type supersonic wind tunnel. The tunnel Mach number can range from 1.5 to 4.0 and has a constant test section area measuring 150 mm x 150 mm in cross section with a length of 650 mm. For the present study, the Mach number was set to 3.0 and a run time of 5 seconds was used beginning once the freestream Mach number was established. The freestream test parameters for the incoming flow have been tabulated in Table 1.

B. Experimental model

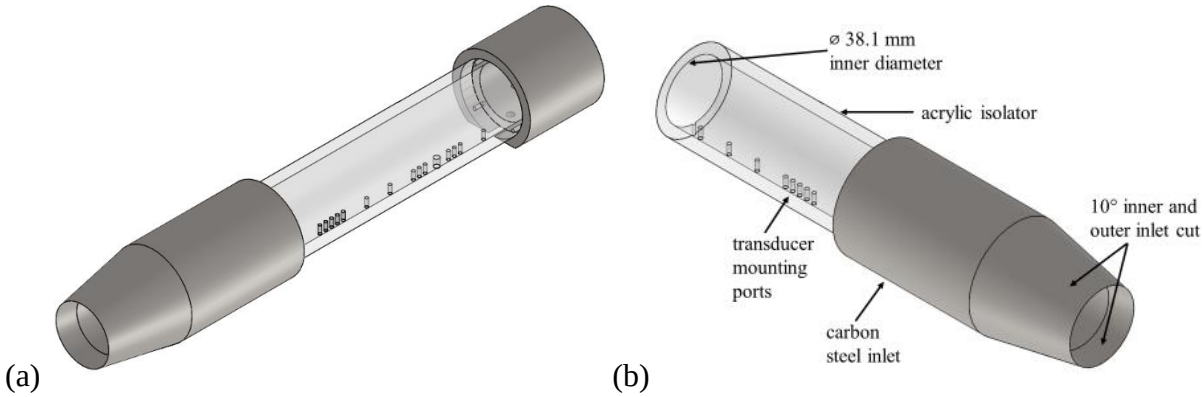

Figure 1: Isometric views of scramjet model (note, (a) full isolator model (b) annotated section view).

The hollow cylindrical isolator model shown in Figure 1(a) was developed to characterize the flowfield leading up to unstart initiation. The assembled isolator has a constant inner diameter of 38.1 mm and total length of 393.6 mm. The forward 10° inlet and the trailing duct were machined from low carbon steel to lengths of 139.6 mm and 50.8 mm, respectively. The central portion of the isolator duct was machined from clear acrylic, such that a large portion of the flowfield was visible for imaging experiments. Pressure transducer ports were made along the bottom centerline of the acrylic portion of the isolator with varied streamwise separation, spanning the majority of the duct. Figure 1(b) is an annotated section view of the model, included to visually mark the important aspects of the model. Both the inlet and duct were machined such that the transparent duct could be mounted to the strut without obstruction. The model was mounted from the tunnel sidewall using the strut, which pushed it an inch towards the centerline of the test section, allowing the flowfield to evolve without significant influence from tunnel sidewall effects.

The jet injection port was located 288.8 mm downstream of the leading edge of the isolator. High-pressure Versilon Polyurethane (C-544-A I.B) tubing with an inner diameter of 3.175 mm was mounted to the injection port, run through the strut, and out a hole machined in the sidewall all such that the test section was entirely sealed. The tubing was then connected to one side of a two-way solenoid (Peter Paul Series 20 Model EH22). The other side of the solenoid was connected to a nitrogen tank with a variable pressure regulator allowing for jet injection pressures up to 600 psig. The solenoid was wired such that the jet would be activated when a switch was flipped. In all experiments using jet injection, the jet was manually started approximately 2.5 seconds after establishment of the test Mach number.

Experiments were conducted for the five jet mass flow ratios presented in Table 2. The mass flow for the jet injection was calculated using the minimum area of the jet injection system (the 2.29 mm inner diameter barbed tube connector used to mount the tubing to the isolator model) and assuming a chocked flow. The isolator's mass flow was computed using the free stream conditions. Jet momentum ratio, J, was calculated according to Im et al. [9] where $J = (\gamma p M^2)_{jet}/(\gamma p M^2)_\infty$.

Table 2: Jet injection cases (note, P_{jet}: gauge pressure from nitrogen tank regulator, $\dot{m}_{jet}$ / $\dot{m}_{isolator}$: mass flow ratio between the jet and freestream, J: jet momentum ratio).

Case	p_{jet} (psig)	$\frac{\dot{m}_{jet}}{\dot{m}_{isolator}}$	J
1	0	0	0
2	100	1.72	3.89
3	250	3.97	8.97
4	400	6.21	14.05
5	600	9.21	20.82

C. Experimental techniques

1) Surface streakline flow visualization

Surface streakline visualization was carried out for all cases to qualitatively identify the mean flow structure of the isolator. A mixture of mineral oil and DayGlo Rocket Red pigment, which fluoresces red under UV light, was used as the visualization medium. The mixture was painted onto the half of the model facing the camera, which was mounted perpendicular to the test section window. The test section was illuminated with an ISSI LED module. Images were recorded at approximately 60 Hz using a Nikon D5200 DSLR camera, equipped with a 590 nm long-pass filter, and time averaged to provide an approximate mean isocontours of the wall shear stress. These streaklines help to locate approximate shock impingement points (identified by accumulation of pigment) and allow qualitative comparison of wall shear stress at different mass flow ratios.

2) Wall static pressure measurements

High-frequency wall static pressure measurements were performed for cases 1 and 2 to obtain a quantitative understanding of the mean and unsteady characteristics of the isolator. High frequency response pressure transducers (Kulite, Inc., model XCQ062-15A) were used for making the measurements. These sensors have a nominal diameter of 1.7 mm, an effective frequency of 50 kHz, and an uncertainty in instantaneous pressure of 1% of p_∞. The transducers were mounted in ports flush with the inner bottom wall of the isolator. Only four transducers could be utilized at a time due to hardware limitations, so separate runs were required to allow

for measurements in all ports. Any transducer port unoccupied by one of the four transducers was filled with a screw so that the entire surface of the inlet was smooth and sealed. The pressure sensor signals were sent through a DL instruments band pass with a cutoff frequency of 50 kHz, then digitized at 100 kHz using an Analog-to-Digital converter (National Instruments, Inc., Model: USB 6366).

III. Results and Discussion

A. Flow visualization

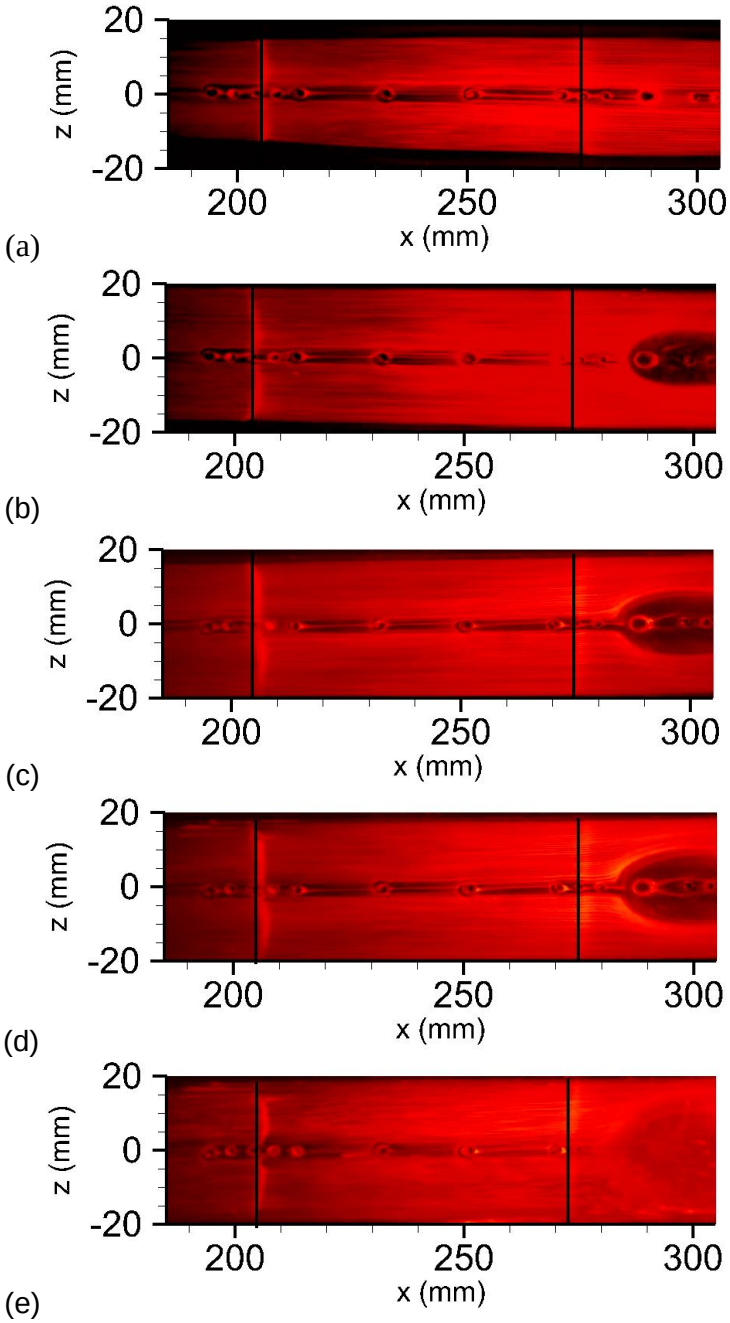

Figure 2: Surface streakline flow visualization (note, (a) through (e) correspond to jet injection cases 1 through 5).

Figure 2 shows the time-averaged streakline visualizations for the five jet injection cases. The flow is from left to right (flow in positive x-direction) and the origin is located at the spanwise center of the isolator leading edge. Figure 2(a) depicts the flow visualization without jet injection. Relatively uniform streaklines can be seen throughout the isolator, which are nominally parallel to the freestream direction. Two distinct shock impingement lines are apparent where pigment has accumulated in vertical lines near x = 204.8 mm and x = 274.5 mm. Black vertical lines were added to demarcate the leading edge of each visible shock impingement location. Due to the length of the isolator preceding the visible section, at least one upstream shock impingement is missed.

The uniform streaklines and shock impingement locations are consistent for all cases. In the cases with jet injection, a clear dispersion of pigment occurs in the wake of the jet. The wake appears to be relatively symmetric about the model centerline. A small upstream influence is seen forward of the injection port with the width of the wake expanding in the downstream direction until a maximum diameter is reached, after which the width remains constant. The maximum wake width is seen to increase proportionally to the jet injection pressure. The wake of the jet in the fifth case, depicted in Figure 2(e) is distorted by pigment splatter on the far side of the isolator, but the edges of the wake are visible. This widening of the jet wake can be associated with the stronger shock that corresponds to larger J ratios.

The flow visualizations for cases 1 and 2 were conducted with slightly different paint mixture of florescent pigment and mineral oil. The different mixtures can cause the movement and accumulation of the paint to vary slightly, which could cause minor differences between the observed impingement lines. Nevertheless, the location of the shocks were tabulated in Table 3 by recording the streamwise location of the black vertical marker lines. No upstream motion of the shock train can be observed at any of the jet injection pressures. All differences seen in the impingement locations are within the variance expected by the varied paint mixtures and minute differences in free stream conditions between runs. The lack of upstream shock train motion suggests that the pressure rise caused by the jet injection is insufficient to significantly separate the boundary layer and allow upstream propagation of information. According to Wagner et al [3], if sufficient back pressure accumulated to initiate the unstart process, the shock trains would weaken and propagate upstream. The consistency between shock impingement locations between case 1, with no jet injection, and all other cases confirms that none of the mass flow ratios were sufficient to unstart the inlet.

Table 3: Shock impingement points measured from flow visualization.

Case	Upstream Shock Impingment (mm)	Downstream Shock Impingment (mm)
1	205.1	274.6
2	204.0	273.6
3	204.6	274.7
4	205.0	275.1
5	204.8	272.8

B. Wall static mean pressure measurements

Figure 3 shows the mean wall static pressure profiles for cases 1 and 2. These are the only two cases for which wall static pressure measurements were recorded. The average values

from three runs, all on the same day, are shown. A dark vertical dashed line is included at x = 288.8 mm to demark the injection port location. The pressures are normalized by the freestream pressure in Table 1. Despite wall static pressure measurements only being conducted on the baseline case and the lowest mass flow ratio of all the jet injection cases, there are still relevant remarks to be made.

The furthest upstream transducer is located a relatively large distance downstream from the leading edge of the isolator at x = 155.4 mm, allowing for at least one shock impingement to occur upstream of the region of data collection, as previously mentioned. This can be observed by the pressure drop seen between the two most upstream transducers, which is caused by impingement of the post-shock expansion. Following this initial drop in mean pressure, two distinct peaks in the mean pressure of the baseline case are seen. The first pressure rise begins at x = 203.0 mm and reaches a peak of $p_w/p_\infty = 2.21$ at x = 212.6 mm. The second pressure spike begins at x = 273.5 mm and peaks at x = 279.2 mm where $p_w/p_\infty = 2.2$. The shock impingement locations, assumed to be where pressure rise is first seen, are both within 1% of the locations recorded in Table 3 from surface streakline visualization, hence that the two methods are in good agreement. The second case, with 100 psig of jet injection shows no indication of upstream shock train motion. It can readily be observed that there is little change in the mean pressures of the two cases upstream of the jet injection. The transducer at x = 298.3 mm (the first one downstream of the jet injection point) observes a significant decrease in mean pressure relative to that seen without jet injection. The mean pressures with jet injection recover slightly but remain lower than the base case for the remainder of the data collection region. This observed pressure decrease is in opposition to the expected pressure response. The transducers are located downstream of strong injection shock and pressures should be elevated. Reasons for this significant discrepancy between expected and measured pressure change are unknown and must be the topic of future investigation.

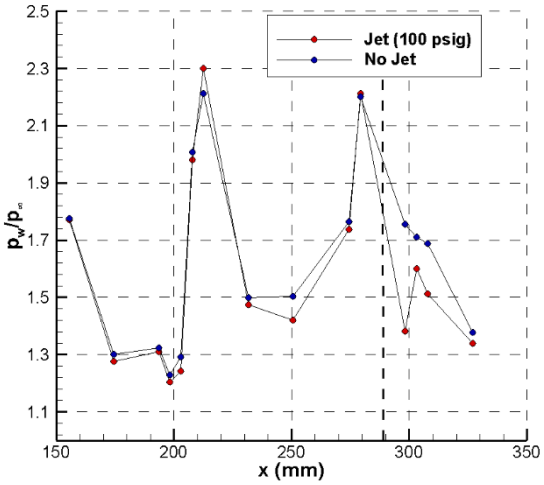

Figure 3: Wall static mean pressure profile for case 1 and 2 (no jet and 100 psig jet configurations).

C. Wall static r.m.s pressure measurements

Figure 4 shows the r.m.s pressure normalized by the local wall static pressure for the first two jet injection cases (no jet and 100 psig jet). The r.m.s pressure was also computed by taking an average over three runs and the injection port is again marked with a dark vertical dashed line. The case without jet injection has three peaks, with the two furthest upstream corresponding to the two shock impingements observed by the flow visualization and mean pressure profiles. The

most downstream peak suggests that there may be a third shock impingement, but no pressure rise is seen in the mean pressure profile. It is feasible that this rise in unsteadiness could be an artifact of the model imperfectly transitioning from the clear acrylic of the duct to low carbon steel. The general trend of increased unsteadiness near shock impingement is in good agreement with the base started flow recorded by Wagner et al [3].

The addition of jet injection does not affect the upstream unsteadiness of the shock train in the isolator as seen by the strong agreement in r.m.s values upstream of x = 288.8 mm. The largest deviation in r.m.s upstream of the jet between the two cases occurs at x = 274.5 where the r.m.s value rises to σ_p/p_w = 0.032, approximately 11.9% greater than that seen without jet injection. The transducer immediately following the jet injection observes a large spike in r.m.s to σ_p/p_w = 0.065, roughly twice that seen at the upstream shock impingement locations. Following this large spike, the r.m.s quickly drops down to approximately the levels seen near prior shock impingements. This is attributed to the transducer sitting within the turbulence of the jet's wake.

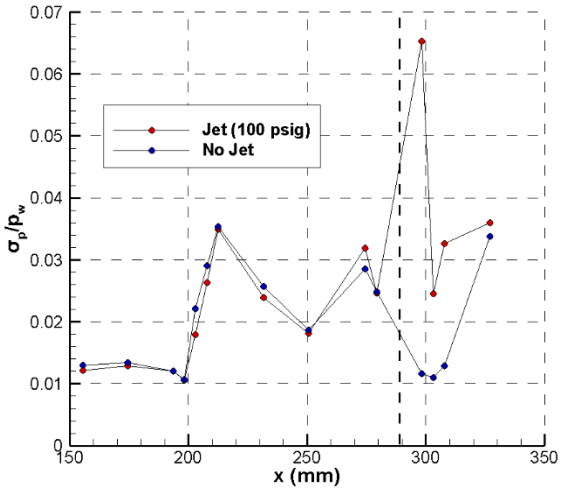

Figure 4: Wall static r.m.s pressure profile for case 1 and 2 which corresponds to no jet and 100 psig jet configurations.

D. Time pressure traces

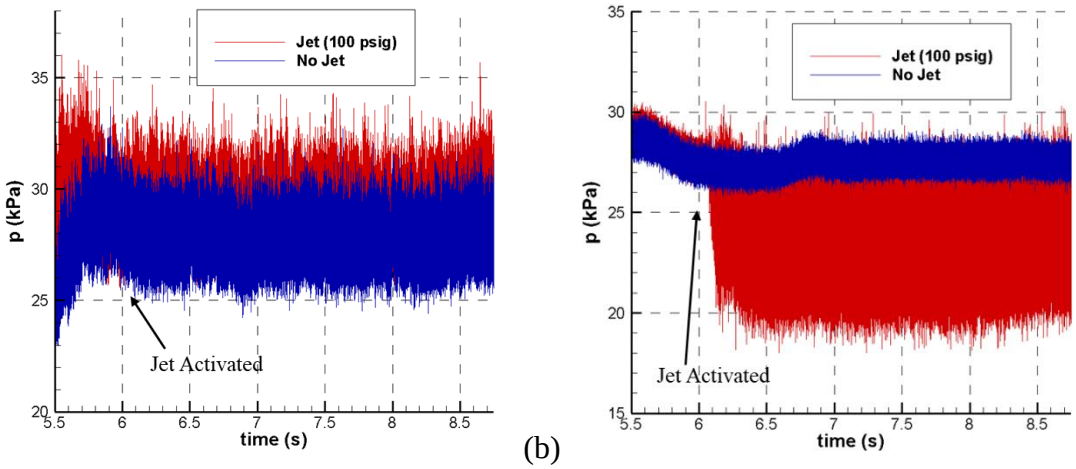

Figure 5: Wall static time pressure traces for cases 1 and 2 (note, (a) x = 274.5 mm (b) x = 298.3 mm).

Time pressure traces are included in Figure 5 to support discussion regarding the unexpected drop in mean pressure associated with jet activation. The pressure time traces are from two runs with the transducers in the same locations, with the first and second runs corresponding to case 1 and 2. The time at which jet injection begins is marked. Figure 5(a)/(b) have a streamwise location of x = 274.5 mm and x = 298.3 mm, respectively, with the former being located at the shock impingement location closest to the injection port and the later located at the first transducer downstream of the injection port. No obvious changes in the time pressure trace upstream of the injection port is observed following the activation of the jet. In contrast, the activation of the jet is largely obvious downstream of the injection port. The response to jet injection downstream is a decrease in the mean pressure and a large increase in the r.m.s value. This agrees with the mean and r.m.s pressure traces and contradicts expectations. Since the main point of mass injection is to raise back pressure, this discrepancy must be explored in future investigations.

E. Wall static pressure power spectra

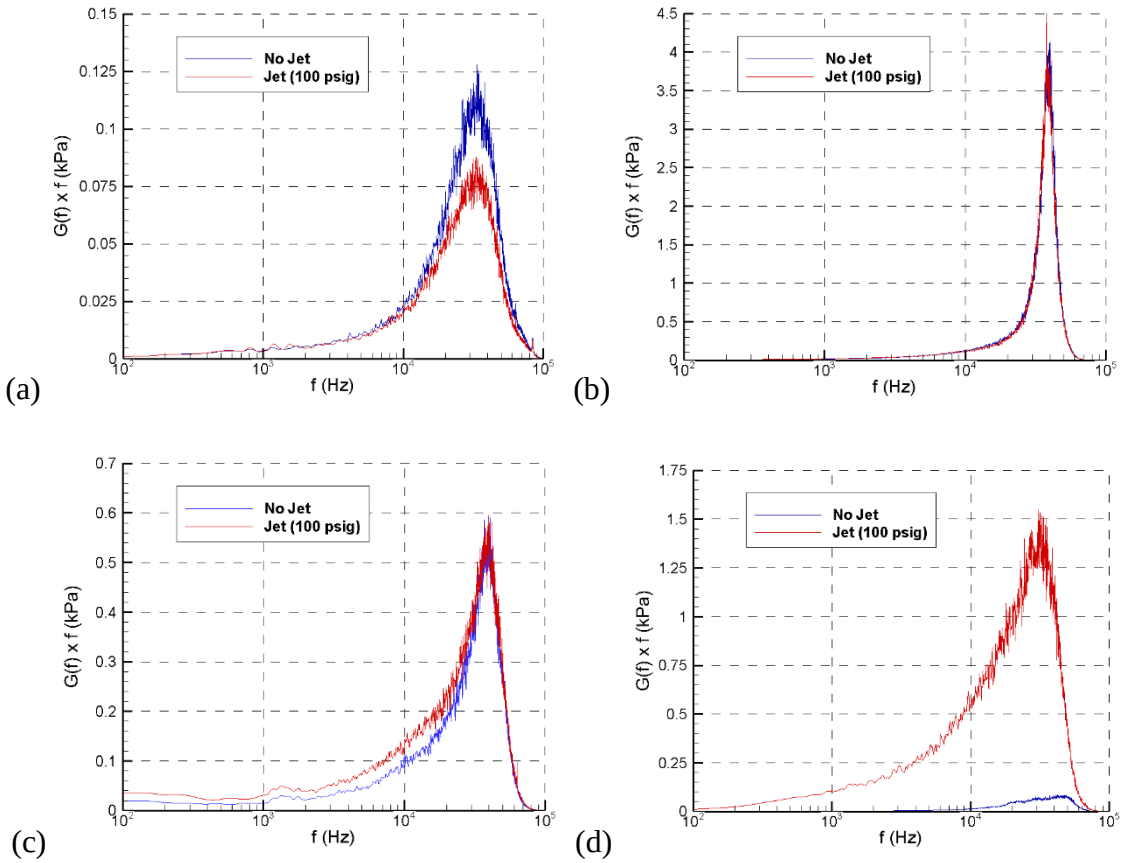

Figure 6: Frequency pre-multiplied power spectra comparison for case 1 and 2 which corresponds to no jet and 100 psig jet configurations (note, (a) x = 155.4 mm (b) x = 212.6 mm (c) x = 274.5 mm (d) = 298.3 mm).

Figure 6 presents the frequency pre-multiplied power spectra from four streamwise locations to provide further insights into the impact which jet injection may have on shock train dynamics. The power spectra is plotted against frequency on a logarithmic scale, which allows for direct comparison of the magnitudes of unsteadiness at any frequency between cases 1 and 2

(no jet and 100 psig jet). An artifact of the 50 kHz low-pass filter in the pressure signal data acquisition system is manifest across all streamwise locations through the steep drop in magnitude at 50 kHz. Figure 6(a) corresponds to x = 155.4 mm and is included as a representation of undisturbed boundary layer. Much of the energy content is contained within the high frequency region (f > 10 kHz). This high frequency region is associated with the passage of boundary layer structures. The dominance of high frequency motion is consistent between both cases, with case 2 exhibiting a slightly lower peak magnitude.

Figure 6(b)/(c) correspond to the transducers which registers the peak σ_p/p_w values in the baseline case, at a streamwise location of x = 212.6 and x = 274.5 mm, respectively. The power spectral density of (b) is highly concentrated around a peak frequency of f = 40.2 kHz which overshadows any low-frequency unsteadiness that may be present. In (c) there is a notable increase in the magnitude of lower frequency unsteadiness. The increase in energy content for frequencies below 10 kHz suggests that the shock train is exhibiting low-frequency unsteadiness. It can also be observed that case 2 (with jet injection) of (c) shows marginally higher magnitudes of lower frequencies, which may indicate a minor increase in low-frequency unsteadiness associated with jet injection at the shock impingement location just upstream of the injection port. Despite the increased magnitude of lower frequencies, the overall power spectral densities are still dominated by high-frequency boundary layer passage.

Figure 6(d) is from a streamwise location of x = 298.3 mm, just downstream of the injection point. There is a large increase in the magnitude of all frequencies in case 2, with jet injection. This observation agrees with the pressure r.m.s values from this streamwise location, where r.m.s values with jet injection jumps to an overall maximum with the baseline case r.m.s value significantly drops. The rise in r.m.s and power spectra levels in case 2 is associated with the high turbulence of the jet injection.

IV. Conclusions

The present study experimentally investigates the mean and unsteady characteristics of a cylindrical isolator for five cases with mild jet injection mass flow ratios, representative of a buildup to unstart initiation. The isolator, with a 10° inlet and a 38.1 mm inner diameter, was placed in a Mach 3.0 flow. Surface streakline visualization qualitatively confirmed that none of the five cases of jet injection unstarted the model and suggested that the shock train upstream of the jet was not noticeable influenced by the downstream mass addition. The effect of increased jet momentum ratio was apparent in the widening of the jet's wake, indicated by the dispersion of the streakline visualization pigment. High-frequency wall static pressure measurements were taken to quantitatively evaluate the mean and unsteady characteristics of the flowfield. The mean pressure profile indicated the presence of at least one shock reflection prior to the measurement zone. The two shock impingements seen in the flow visualization were confirmed by distinct mean pressure rises which began at the transducer nearest the location identified by the flow visualization. No notable mean or unsteady differences upstream of the jet injection port were observed between the baseline case and cases with jet injection. Downstream of the injection port, with a 100 psig jet, the transducers within the wake experienced relative pressure drops and increased unsteadiness. The decrease in mean pressure and significant increase in pressure r.m.s values was confirmed by time pressure traces. The reason for the counterintuitive mean pressure drop is unknown and must be explored in future work. The frequency pre-multiplied power spectra showed small magnitudes of low-frequency unsteadiness from shock oscillations but an overall dominance of high frequencies, associated with turbulent boundary layer passage. This

initial exploration of a cylindrical isolator experiencing mild mass injection will be instrumental to future investigation of the model with mass flow ratios sufficient to initiate the unstart process.

References

[1] A. Wieting, "Exploratory study of transient unstart phenomena in a three-dimensional fixed-geometry scramjet engine," NASA, Hampton, Va, 1976.

[2] A. Church, "Air Force World, Second X-51 Test Cut Short," *Air Force magazine,* vol. 94, pp. 17-18, 2011.

[3] J. Wagner, K. Yuceil, A. Valdivia, N. Clemens and D. Dolling, "Experimental investigation of unstart in an inlet/isolator model in Mach 5 flow," *AIAA,* vol. 47, no. 6, pp. 1528-1542, 2009.

[4] S. O'Bryne, M. Doolan, S. Olsen and A. Houwing, "Analysis of transient thermal chocking process in a model scramjet engine," *Propulsion and Power,* vol. 16, no. 5, pp. 808-814, 2000.

[5] S. Laurence, S. Karl, M. Schramm and K. Hannemann, "Transient fluid-combustion phenomena in a model scramjet," *Fluid Mechanics,* vol. 722, pp. 85-120, 2013.

[6] S. Im and H. Do, "Unstart phenomena induced by flow choking in scramjet inlet-isolators," *Progress in Aerospace Sciences,* vol. 97, pp. 1-21, 2018.

[7] E. Curran, W. Heiser and D. Pratt, "Fluid phenomena in scramjet combustion systems," *Fluid Mechanics,* vol. 28, pp. 323-360, 1996.

[8] H. Do, S. Im, M. Godfrey Mungal and M. Cappelli, "Supersonic inlet duct unstart induced by fuel jet injection," in *International Symposium on Turbulance and Shear Flow Phenomena*, 2011.

[9] S. Im, D. Baccarella, B. McGann, Q. Liu, L. Wermer and H. Do, "Unstart phenomena induced by mass addition and heat release in model scramjet," *Fluid Mechanics,* vol. 797, pp. 604-629, 2016.

[10] K. McDaniel and J. Edwards, "Three-dimensional simulation of thermal choking in a model scramjet combustor," in *AIAA*, Reno, NV, 2001.